POLITECNICO
MILANO 1863

SCUOLA DI INGEGNERIA INDUSTRIALE
E DELL'INFORMAZIONE

Executive Summary of the Thesis

Understanding friction drag reduction via synthetic forcing

Laurea Magistrale in Aeronautical Engineering - Ingegneria aeronautica

Author: Andrea Conforti

Advisor: Prof. Maurizio Quadrio

Co-advisors: Ing. Federica Gattere; Dott. Alessandro Chiarini

Academic year: 2022-2023

1. Introduction

In the context of active control techniques for a turbulent channel flow, one of the most widely studied and used techniques is certainly spanwise wall oscillation, where the wall oscillates with a sinusoidal motion:

$$W(y=0,t) = A\sin\left(\frac{2\pi}{T}t\right), \qquad (1)$$

where $W(0,t)$ represents the spanwise component of the mean velocity vector at the wall, t is time, y is the wall-normal coordinate, A is the oscillation amplitude, and T is the oscillation period. Both numerical simulations and experimental studies [4] have documented a reduction in friction provided by this technique. When the wall oscillates (Eq. (1)) a transverse boundary layer (the so-called Stokes layer) is created, whose velocity profile $W(y,t)$ is known and equal to the analytical solution of the second Stokes problem. This profile is completely determined, both in its spatial and temporal evolution, by the value of the oscillation period T that governs the wall motion. An extensive literature has highlighted that the value of this parameter that guarantees the greatest Drag Reduction (DR) percentage is $T^+_{opt} = 100$ (where the superscript $+$ is used to indicate a scaled quantity in viscous units). The meaning of this value, despite some attempts to explain it, remains quite unclear. Indeed, as previously mentioned, this parameter T is responsible for both the temporal frequency of the Stokes layer oscillations and the spatial thickness of the velocity profile inside it, namely $\delta = \sqrt{T\nu/\pi}$ (being ν the kinematic viscosity of the fluid). Therefore, it is important to understand whether this $T^+_{opt} = 100$ is optimal because it ensures that specific temporal frequency, or if it is only the best compromise between temporal and spatial behavior.

2. Objective

The goal of this study is to improve the understanding of skin friction reduction caused by oscillating wall technique. Specifically, it is a matter of understanding the true meaning of the wall oscillation period T. In order to overcome this challenge, it is proposed a new approach that directly imposes the transverse velocity profile of the Stokes layer on the flow, separating the spatial and temporal variations by making δ and T indipendent, as follow:

$$W(y,t) = A\exp\left(-\frac{y}{\delta}\right)\sin\left(\frac{2\pi}{T}t - \frac{y}{\delta}\right). \qquad (2)$$

Through a parametric DNS study of a turbulent channel flow, it is possible to examine the pre-

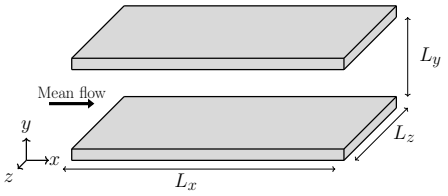

Figure 1: Schematic geometry of a plane channel flow.

cise impacts of temporal and spatial variations in the spanwise forcing profile on DR. Therefore, once the friction reduction map varying with T and δ is known, the effects of these parameters on the flow will be investigated through analysis of Reynolds stresses and, in general, through observation of the behavior of ideal tracers inserted at the beginning of the simulations.

3. Method

This study uses a pseudo-spectral DNS code to solve the incompressible Navier-Stokes equations for turbulent channel flow, utilizing fourth-order-accurate compact finite-difference schemes in the wall-normal direction y and Fourier expansions for high resolution and efficiency in parallel computing in the homogeneous directions x and z. In order to study the effects of the Stokes layer parameters T and δ, the transverse velocity profile $W(y,t)$ (Eq. (2)) is directly imposed on the flow, keeping the wall still. From a computational perspective, this means assigning the spanwise velocity profile $W(y,t)$ upstream of the convolution calculations at each time step, in order to ensure that the interaction of all modes takes place with the intended mean profile.

3.1. Simulations parameters

The simulations are conducted with Constant Flow Rate (CFR) at a Reynolds number $Re = U_p h/\nu = 10500$ (where U_p is the centerline velocity of a laminar Poiseuille flow with the same flow rate), which corresponds to $Re_\tau = u_\tau h/\nu = 400$ in the unforced case (where h is half the distance between the channel walls, and u_τ is the friction velocity of the uncontrolled case). The size of the computational box is $(L_x, L_y, L_z) = (4\pi h, 2h, 2\pi h)$, discretized with $N_y = 300$ grid points in the wall-normal direction, and $N_x = 256$ and $N_z = 256$ Fourier modes in the x and z directions respectively. The mesh in the wall-normal direction uses a constant-linear nodes distribution, maintaining $\Delta y^+_{min} = 0.5$ until $y^+ < 25$, after which Δy^+ increases linearly until achieving $\Delta y^+_{max} \approx 6.2$ at the channel centerline. The simulations are run for 10,000 time steps with $\Delta t^+ \approx 0.15$, starting from a well-developed flow condition. The study aims to investigate the effect of the parameters pair (T^+, δ^+) on the friction coefficient C_f. The changes in C_f are measured as a percentage with respect to the friction coefficient of the reference case $C_{f,0}$ through DR(%) parameter, which corresponds to the percentage reduction in the energy required to drive the fluid in the streamwise direction at a fixed flow rate (CFR).

3.2. Stokes layer inputs

The primary simulations aim to apply different combinations of $W(y,t)$ for different pairs of (T^+, δ^+) values, and then analyze the resulting DR(%) for each case. The amplitude of the forcing oscillation was set to $A^+ = 12$. The range of oscillation periods considered are $T^+ = 25-200$, with a ΔT^+ of 25 between each value. An additional value of $T^+ = 10$ was chosen to represent a low-period case. The range of δ^+ investigated is $\delta^+ = 2 - 20$, with a $\Delta\delta^+ = 2$, to test velocity profiles which perturb near wall structures at different wall-normal locations. For each value of T^+, simulations of the canonical Stokes layer were also performed, where $\delta^+ = \sqrt{T^+/\pi}$. In total, 92 simulations were carried out for the different (T^+, δ^+) pairs, in addition to a reference simulation of the unforced flow.

4. Drag reduction results

Figure 2 shows that oscillating wall technique, which results in all (T^+, δ^+) pairs identified by the black line, is limiting in terms of DR. The previous analyses that designated $T^+ = 100$ as the optimal value for the forcing period were biased because a certain T^+ corresponded to a fixed δ^+, preventing separate evaluations of the spatial and temporal contributions. Thus, the value of $T^+_{opt} = 100$ does not hold any significant meaning, and smaller periods show the potential to increase DR(%) by 40%, if δ^+ can be arbitrarily chosen. In fact, while staying on the black line $DR_{max}(\%) = 28.3$ for $T^+ = 100$, a value of $DR_{max}(\%) \approx 40$ can be reached with the velocity profile with $(T^+_{opt}, \delta^+_{opt}) = (40, 12)$.

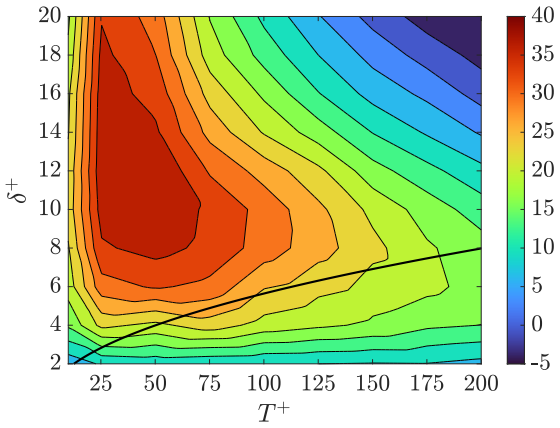

Figure 2: DR(%) for different (T^+, δ^+) pairs in reference scaling (at Nominal $Re_\tau = 400$ and $A^+ = 12$). Black line is the true Stokes layer ($\delta = \sqrt{T\nu/\pi}$).

Focusing initially on the oscillation period, this value of T^+_{opt} is not random or meaningless: in fact, $T^+_{opt} = 40$ had already been identified as the Lagrangian time scale representing a typical survival time of the statistically significant turbulent structures by [3]. It seems that when T^+ is larger than the optimum, the near-wall streaks are given enough time to establish their internal dynamics between successive Stokes layer cycles. However, when $T^+ \simeq T^+_{opt}$, the forcing time aligns with the characteristic time of streak dynamics and effectively disrupts the streaks, preventing them from adjusting to their natural life cycle. Conversely, the absolute DR_{max} is obtained for $\delta^+ = 12$, but it cannot be said that this δ^+ value represents the optimum for all oscillation periods. Indeed, as T^+ deviates from T^+_{opt}, it can be observed that δ^+_{opt} gradually decreases. Anyway, $\delta^+_{opt} = 12$ is not an unexpected value, since it is well established that the dinamically relevant turbulent structures are located at a height of $y^+ \approx 12$ from the wall. If these specific structures are forced with T^+_{opt}, it is effective if the transverse boundary layer includes these streaks. On the other hand, if the period T is far from the optimal one, the best DR result is obtained when the Stokes layer remains slightly closer to the wall, only tilting the streaks in the viscous sublayer, which seem to be much less dependent on the T value. This statement is confirmed by looking at the DR results for $\delta^+ = 2$, where a sort of independence of DR with respect to T^+ is clearly visible. Similarly, a certain independence of DR with respect to δ^+, can be noticed from Fig. 2 at very low periods as $10 \leq T^+ \leq 20$. These observations can be explained by the fact that when the value of δ is small, the Stokes Layer does not interact much with the wall cycle, because it is located very close to the wall, without affecting those structures that are more responsible for turbulent production. At the same time, when the period T is very small, it does not interact with the regeneration cycle of turbulent structures at wall. This may explain why in both cases there appear to be a certain independence of DR with respect to the forcing parameters.

5. Reynolds stresses analysis

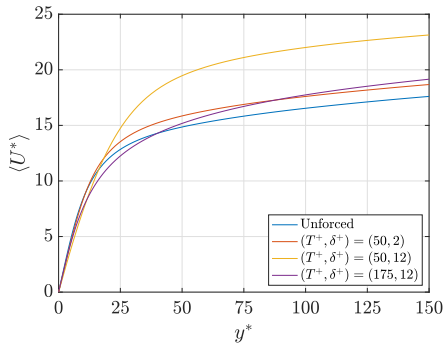

(a)

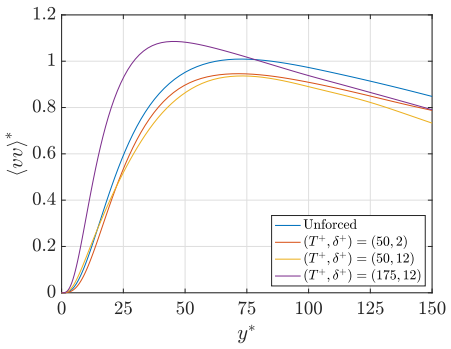

(b)

Figure 3: Wall normal profile of mean streamwise velocity (a) and vertical Reynolds stresses (b) (at Nominal $Re_\tau = 400$ and $A^+ = 12$).

All variables shown in this analysis are scaled in actual viscous units ($*$ superscript), therefore considering each case with respect to its viscous units. The quantities enclosed in the $\langle \cdot \rangle$ brackets are temporally and spatially averaged along the homogeneous x and z directions.

In order to find a physical explanation to the results shown in Fig. 2, it is interesting to observe how the Reynolds stresses behave under different forcing condition with respect to the reference unforced case. Three different forcing conditions are analyzed, corresponding to three different (T^+, δ^+) pairs, appropriately chosen: $(50, 2)$, $(50, 12)$, and $(175, 12)$, which result in a DR(%) of $10.5\%, 39.4\%$, and 13.8%, respectively. Figure 3a shows the wall-normal behavior of the mean velocity $\langle U^*(y^*)\rangle$ for different forcing conditions, where it can be seen that the linear near-wall trend of the mean velocity extends to higher values of y^* for the forcing that ensures better DR, namely $(50, 12)$. Consequently, the present results provide further evidence [1] that an increase in DR is connected to a thickening of the viscous sublayer, regardless the specific values of T and δ, as exemplified by the cases of $(T^+, \delta^+) = (50, 2)$ and $(T^+, \delta^+) = (175, 12)$ respectively, where the thickening is also present, but way less than with $(50, 12)$.
Figure 3b illustrates the variation of $\langle vv\rangle^*$ along the wall-normal direction, which reflects the intensity of ejections/sweeps phenomena. While $\langle vv\rangle^*$ is attenuated for the forcings with $T^+ = 50$, this is not observed for the one at $T^+ = 175$, and instead there is even an increase in $\langle vv\rangle^*$ for $y^* \leq 75$ compared to the unforced case. The aforementioned behavior can be clarified by examining the results presented in Figures 4a, 4b, and 4c, in which the pressure-strain correlation terms are shown. These terms are responsible for the energy transfer between diagonal Reynolds stresses due to the effects of pressure-strain interactions, and determine their relative magnitudes. Specifically, when $\Pi_{ii} < 0$ (where i can range from 1 to 3, corresponding to the streamwise x, wall-normal y, and spanwise z directions, respectively), energy is transferred from $\langle u_i u_i\rangle$ to the other diagonal Reynolds stresses, and vice versa when $\Pi_{ii} > 0$. The behaviour of Π^*_{11} (Fig. 4a) shows that there is no inhibition of energy exchange between $\langle uu\rangle^*$ towards $\langle vv\rangle^*$ and $\langle ww\rangle^*$ in the cases of $(50, 12)$ and $(175, 12)$ forcings: instead, even more energy is transferred with respect to the reference case (because of a more pronunced negative peak). The difference between these two forcings in the redistribution patterns can be easily identified by examining Π^*_{22} and Π^*_{33} curves (Figures 4b and 4c).

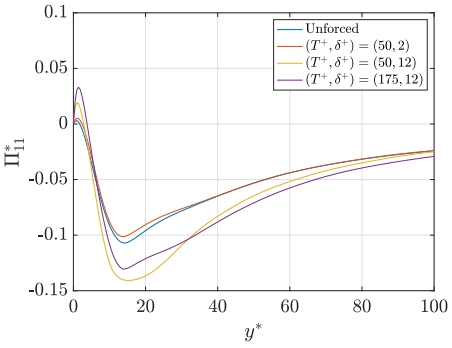

(a)

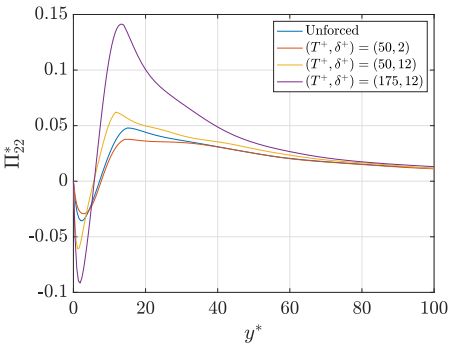

(b)

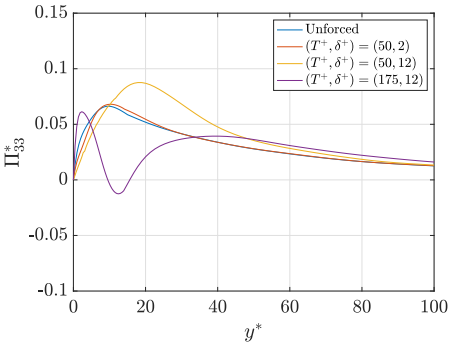

(c)

Figure 4: Wall normal profiles of pressure-strain correlation terms (at Nominal $Re_\tau = 400$ and $A^+ = 12$): (a) Π^*_{11}; (b) Π^*_{22}; (c) Π^*_{33}.

In comparison to the unforced case, two opposite behaviors are observed: for the $(50, 12)$ forcing, most of the energy seems to follow a preferential path from $\langle uu^*\rangle$ to $\langle ww\rangle^*$, while the opposite behavior is observed for the $T^+ = 175$ forcing, where a lot of energy goes from $\langle uu^*\rangle$ to $\langle vv\rangle^*$, since Π^*_{22} dominates and Π^*_{33} even shows a negative peak, suggesting that some energy is also transferred from $\langle ww\rangle^*$ to the wall normal stress $\langle vv\rangle^*$. At this point, the reason for

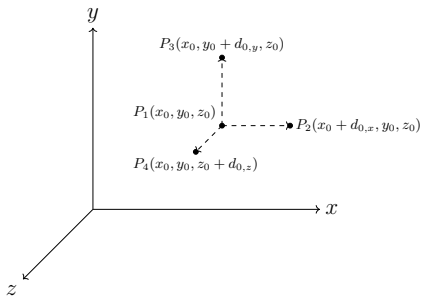

Figure 5: Initial positioning of a group of particles.

the greater value of $\langle vv \rangle^*$ for the $T^+ = 175$ forcing can be somehow supported by evidence from the budget terms Π_{ii}. The observation of an increased energy exchange from $\langle uu^* \rangle$ to $\langle vv^* \rangle$ when $T^+ = 175$, provides evidence that there is no inhibition of the vertical fluctuating velocity field. On the contrary, our findings suggest that sweep and ejection events may be enhanced by slow-oscillations of the Stokes layer.

6. Particles tracking

6.1. Computational method

This additional analysis aims to investigate the behavior of a turbulent channel flow under different forcing conditions, introducing ideal tracers into the computational domain. After setting the total number of particles n_p, particles are organized into $n_{group} = n_p/4$ groups of four, as shown in Figure 5. The first particle of each group, labeled as P_1, is inserted at a specific point $\mathbf{x}_0^{P_1} = (x_0, y_0, z_0)$ in the domain at time $t = 0$, while the other three particles, namely P_2, P_3 and P_4 are introduced at same position but shifted by a certain $d_{0,x}, d_{0,y}$ and $d_{0,z}$, respectively. The initial position $\mathbf{x}_0^{P_1} = (x_0, y_0, z_0)$ and the components of the initial separation vector $\mathbf{d}_0 = (d_{0,x}, d_{0,y}, d_{0,z})$ are freely selectable. Once these two inputs, along with the number of four-particle groups n_{group} (and therefore the total number of tracers as $n_p = 4 \cdot n_{group}$) are chosen, the entire process of polynomial interpolation can start. The DNS code affords access to the Eulerian velocity $\mathbf{u}(t)$ for each point of a three-dimensional numerical grid at every time step, which is different to the lagrangian particle's velocity $\mathbf{v}(t)$. As a result, proper interpolation of the particle's Lagrangian velocity $\mathbf{v}(t)$ is needed. In the present work, sixth-order Lagrange polynomials are used as the interpolating function for the discrete velocity field. As a result, the Lagrangian velocity of the particle $\mathbf{v}(\mathbf{x}(t), t)$ is calculated. Then, the position of the i-th particle can be calculated as follow:

$$\mathbf{x}^i(t + \Delta t) = \mathbf{x}^i(t) + \Delta t \cdot \mathbf{v}(\mathbf{x}^i(t), t), \quad (3)$$

where Δt is the chosen time step. In this context, a total of $n_p = 2.2 \cdot 10^6$ particles are released on a plane parallel to the wall for each simulation, in such a way that the entire x-z plane is adequately filled with a sufficient number of tracers. Particle pairs are injected at a release height of y_0^+ with an initial separation of d_0 in various directions. The wall-normal injection height of the particles has been set to $y_0^+ = \delta^+/2$ for each forced simulation, while in the reference case $y_0^+ = 6$. The magnitude of the initial separation vector $\mathbf{d}_0$ has been kept constant at $d_0^+ = 0.76$ or $d_0 = 0.019h$ in all directions. The temporal evolutions of the results will be visualized through the normalized time t with respect to the crossing time τ_{ct}, which in the current simulations (expressed in nominal viscous units) is equal to $\tau_{ct}^+ = L_x^+/u_{cl}^+ \approx 250$, where u_{cl}^+ is the longitudinal velocity at channel centerline. To collect statistical data and perform ensemble averaging, a time window of duration ΔT^+ was used. This time window is expressed in terms of the number of crossing times τ_{ct}^+, and is equal to $\Delta T^+ = 8.5\tau_{ct}^+$.

7. Particles' results

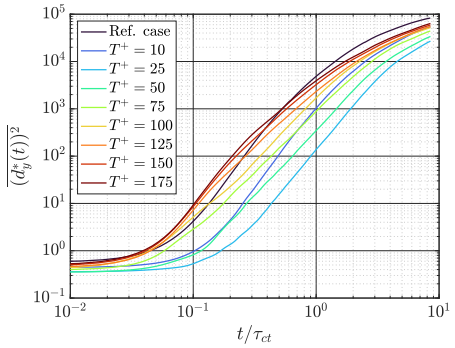

Figure 6: Time evolution of wall-normal relative dispersion due to wall-normal initial separation for different T^+ values.

In this section, it is investigated whether Stokes layer which leads to a higher DR(%), also re-

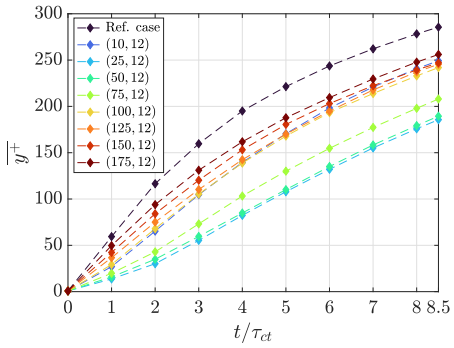

Figure 7: Time variation of the average wall-normal position of all injected particles for different forcings.

sults in a more pronounced blocking effect of vertical velocity fluctuations. In order to analyze the shear sheltering provided by the Stokes layers, it is useful to look at the component of relative dispersion normal to the wall, namely $\overline{d_y^2(t)} = \overline{(y^{P_1} - y^{P_2})^2}$ (where y^{P_1} and y^{P_2} are the wall-normal coordinates of a particles pair, and the overline represents the averaging operation over all particles) [2]. Figure 6 shows wall-normal relative dispersion $\overline{(d_y^*(t))^2}$ due to wall-normal initial separation ($d_{0,y}^+ = 0.76$) with release height $y_0^+ = 6$ for distinct Stokes layers, specifically characterized by same $\delta^+ = 12$ but different T^+. From Fig. 6, it is immediately noticeable that the great majority of forcing conditions reduce $\overline{d_y^*(t))^2}$ compared to the unforced reference case. Essentially, the optimal T^+ order found in the drag reduction analysis (Fig 2) is confirmed. Specifically, the minimum average vertical dispersion is obtained for $T^+ = 25$, followed by $T^+ = 50$ case. This suggests that at these oscillation periods, the Stokes layer is highly effective in reducing vertical fluctuations, resulting in the inhibition of turbulent phenomena such as sweeps and ejections. Fig. 13 shows the average $\overline{y^+}$ position of the particles as a function of time for all forcings at the same $\delta^+ = 12$ and different T^+. After $t = \tau_{ct}$, $\overline{y^+}$ for $T^+ = 25 - 50$ settles at values of 14 and 15 respectively, whereas the reference case provides $\overline{y^+} = 60$. This indicates that, on average, the particles are distributed closer to the wall by about 75% when subjected to the shear induced by the Stokes layer, which therefore has a massive influence on the wall turbulence. As T^+ increases, the effect of shear sheltering persists, albeit to a lesser extent, as the oscillations of the Stokes layers become slower.

8. Conclusions

In conclusion, this study proposes a novel approach to understand the skin friction reduction phenomenon induced by transverse forcing. By decoupling the spatial and temporal variations of the velocity profile into two parameters, δ and T, this study reveals that the temporal variation of the Stokes layer dominates the resulting skin friction reduction. Moreover, the real optimal value of T_{opt}^+ for maximum skin friction reduction is found to be significantly smaller than the one traditionally found in wall motion techniques. These oscillations of the Stokes layer with T_{opt}^+ seem to dampen the vertical fluctuations occurring within the boundary layer, which leads to a reduction in the intensity of sweep and ejection phenomena. As a result, these findings provide valuable insights for the optimization of future drag reduction strategies.

9. Bibliography

References

[1] D. Gatti and M. Quadrio. Reynolds-number dependence of turbulent skin-friction drag reduction induced by spanwise forcing. *J. Fluid Mech.*, 802:553–58, 2016.

[2] E. Pitton, C. Marchioli, V. Lavezzo, A. Soldati, and F. Toschi. Anisotropy in pair dispersion of inertial particles in turbulentchannel flow. *Physics of Fluids*, 24(073305):1–26, 2012.

[3] M. Quadrio and P. Luchini. Integral time-space scales in turbulent wall flows. *Physics of Fluids*, 15(8):2219–2227, 2003.

[4] P. Ricco, M. Skote, and M. A. Leschziner. A review of turbulent skin-friction drag reduction by near-wall transverse forcing. *Progress in Aerospace Sciences*, 123:100713, May 2021.